Dalton Transactions

RSC Publishing

PAPER

View Article Online
View Journal | View Issue

A comparison of sensitized Ln(III) emission using pyridine- and pyrazine-2,6-dicarboxylates – part II†

Cite this: *Dalton Trans.*, 2013, **42**, 2075

Evan G. Moore,*[a,b,c] Jakob Grilj,[d] Eric Vauthey[d] and Paola Ceroni[b]

The synthesis, X-ray structures and photophysical properties of several new Ln(III) complexes with the dianion of pyrazine-2,6-dicarboxylic acid (H_2PYZ) that demonstrate excellent stability and solubility in non-aqueous solution are reported, and compared to structurally analogous complexes derived from pyridine-2,6-dicarboxylic acid (H_2DPA). The Eu(III) and Yb(III) complexes demonstrate efficient metal centered luminescence in the visible and Near Infra-Red (NIR) regions, respectively. Low temperature (77 K) phosphorescence measurements using the corresponding Gd(III) complex has allowed the photophysical properties of the sensitizer to be rationalized, together with corresponding TD-DFT studies for a model complex. Lastly, we have evaluated the sensitization efficiencies for these complexes, and have undertaken femtosecond transient absorption (TA) measurements in order to evaluate the relative importance of the intersystem crossing and energy transfer processes involved with sensitized Ln(III) emission *via* the antennae effect.

Received 24th September 2012,
Accepted 6th November 2012

DOI: 10.1039/c2dt32229c

www.rsc.org/dalton

Introduction

The development of trivalent lanthanide complexes with useful luminescence properties continues to attract considerable research interest, in particular due to their use as emissive probes in biotechnology[1] and for the detection of important biomolecules.[2,3] Emissive Ln(III) cations are particularly suitable for this task, as they are typically insensitive to quenching by oxygen, they possess sharp and characteristic emission spectra, and they demonstrate large 'apparent' Stokes shifts (*i.e.* the difference between excitation and emission wavelength). Additionally, their long lived luminescence allows both spectral and time resolved discrimination of their emission using time gated detection techniques, allowing the luminescent signal to be readily discriminated from that of organic fluorophores, background autofluorescence, and scattered excitation.[4]

We have recently reported[5] the structural and luminescent properties of an Eu(III) complex with pyrazine-2,6-dicarboxylic acid (H_2PYZ, Chart 1). This ligand is an analogue of the very well known pyridine-2,6-dicarboxylic acid or 'dipicolinic acid' (H_2DPA, Chart 1), which is an efficient sensitizer for Ln(III) luminescence.[6] In fact, the Tb(III) and Eu(III) complexes of this ligand have been proposed as useful secondary standards for the quantum yield determinations of Ln(III) complexes.[7,8] We demonstrated that the PYZ^{2-} dianion is also an efficient sensitizer for Eu(III), forming a highly luminescent $Cs_3[Eu(PYZ)_3]\cdot 7H_2O$ complex in the solid state. However, in dilute aqueous solution, the isolated complex rapidly hydrolyses, resulting in a loss of metal centered emission.

Our continued interest in the H_2PYZ ligand as a sensitizer for Ln(III) luminescence stems from initial earlier reports[9] that the S_1 (n–π^*) excited state of pyrazine has a higher intersystem crossing quantum yield ($\Phi_{isc} \sim 1.0$) when compared to pyridine ($\Phi_{isc} \sim 0.3$). As is often the case, if Ln(III) sensitization is assumed to proceed *via* the lowest energy T_1 triplet state of the ligand, then the overall sensitization efficiency, η_{sens}, is a function of Φ_{isc}, and η_{eet}, the efficiency of the ligand-to-metal energy transfer; $\eta_{sens} = \Phi_{isc}\,\eta_{eet}$. Accordingly, since $\Phi_{total} = \eta_{sens}\,\Phi_{Ln}$, we expected that the Ln(III) complexes derived from H_2PYZ would show improved luminescence. In the solid state,

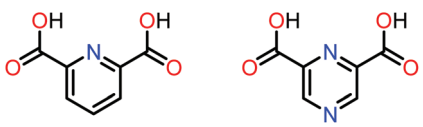

Chart 1 Chemical structures of H_2DPA (left) and H_2PYZ (right) ligands.

[a]*School of Chemistry, University of Melbourne, VIC, 3010, Australia*
[b]*Dipartimento di Chimica "G. Ciamician", Università di Bologna, Via Selmi, 2, Bologna, 40126, Italy*
[c]*School of Chemistry and Molecular Biosciences, University of Queensland, QLD, 4072, Australia. E-mail: egmoore@uq.edu.au; Fax: +61 (0)7 3365 4273; Tel: +61 (0)7 3365 3862*
[d]*Physical Chemistry Department, Sciences II, University of Geneva, 30, Quai Ernest Ansermet, CH-1211 Geneva 4, Switzerland*

†Electronic supplementary information (ESI) available: Additional figures, tables and luminescence spectra. CCDC 902250 and 902251. For ESI and crystallographic data in CIF or other electronic format see DOI: 10.1039/c2dt32229c

This journal is © The Royal Society of Chemistry 2013

this assumption was proven valid, although only a very modest improvement was observed.[5]

In order to complete our analysis of the sensitization processes involved with these isostructural compounds in solution, it was necessary to undertake measurements in non-aqueous solution, to avoid competitive ligand hydrolysis. To this end, we have prepared a new series of complexes with improved solubility in organic solvents, to allow spectroscopic measurements, which we achieved by synthetic substitution of the alkali metal with the tetramethylammonium cation. Herein, we report the X-ray crystal structures for two pseudo-polymorphs of the $(Me_4N)_3[Eu(PYZ)_3]$ complex, which differ in their solvation with either H_2O or MeOH. A corresponding Gd (III) complex has been prepared, in order to evaluate the relative position of the ligand based energy levels, and facilitating a comparison of these results with TD-DFT calculations. Additionally, we have prepared and characterized a $[Yb(PYZ)_3]^{3-}$ complex, which displays sensitized Near Infra-Red (NIR) emission at *ca.* 1 μm, the intensity of which was found to be considerably higher than that of the analogous $[Yb(DPA)_3]^{3-}$ complex. Lastly, we report our initial results using femtosecond transient absorption measurements with this family of compounds, which has enabled an evaluation of the relative kinetics for intersystem crossing and energy transfer involved with the antennae effect after ligand based excitation.

Experimental

General

All solvents for reactions were used as supplied. Pyrazine-2,6-dicarboxylic acid (H_2PYZ) was prepared using literature methods.[10,11] Pyridine-2,6-dicarboxylic acid (H_2DPA) and high purity (>99.9%) $LnCl_3{\cdot}xH_2O$ salts (Ln = Eu, Yb; (x = 5), or Gd; (x = 6)) were used as supplied by Sigma Aldrich (Castle Hill, Australia). Elemental analyses were performed by Microanalytical Services at the School of Chemistry and Molecular Biosciences, University of Queensland, Australia.

Synthesis of complexes

The required complexes were prepared using the following general procedure. A solution of the H_2PYZ or H_2DPA ligand (0.1 mmol) in MeOH (20 mL) was neutralized to *ca.* pH 6 (pH indicator paper) with 30% Me_4NOH. To the resulting cloudy solution was added 0.35 equivalents of $LnCl_3{\cdot}xH_2O$ (Ln = Eu, Yb; (x = 5), or Gd; (x = 6)), and the resulting clear solutions were refluxed for 2 hours. The $[Ln(DPA)_3]^{3-}$ complexes precipitated upon cooling this solution to room temperature. For the $[Ln(PYZ)_3]^{3-}$ complexes, dropwise addition of Et_2O was required to induce precipitation. The resulting white solids were collected and dried by vacuum filtration, with yields of 50–80%. Anal. Calc'd (Found) for $(Me_4N)_3[Ln(PYZ)_3]$ complexes: $EuC_{30}H_{42}N_9O_{12}{\cdot}13H_2O$ (1106.88 g mol^{-1}): C, 32.55 (32.54); H, 6.19 (6.53); N, 11.39 (11.12). $GdC_{30}H_{42}N_9O_{12}{\cdot}9H_2O$ (1040.11 g mol^{-1}): C, 34.64 (34.79); H, 5.81 (5.66); N, 12.12 (11.85). $YbC_{30}H_{42}N_9O_{12}{\cdot}8H_2O$ (M_r = 1037.88 g mol^{-1}): C, 34.72 (34.46); H, 5.63 (5.21); N, 12.15 (12.09). Anal. Calc'd (Found) for $(Me_4N)_3[Ln(DPA)_3]$ complexes: $EuC_{33}H_{45}N_6O_{12}{\cdot}6H_2O$ (977.81 g mol^{-1}): C, 40.54 (40.12); H, 5.88 (5.81); N, 8.59 (8.41). $GdC_{33}H_{45}N_6O_{12}{\cdot}6H_2O$ (983.09 g mol^{-1}): C, 40.32 (40.10); H, 5.84 (5.73); N, 8.55 (8.55). $YbC_{33}H_{45}N_6O_{12}{\cdot}7H_2O$ (1016.90 g mol^{-1}): C, 38.98 (38.83); H, 5.85 (5.27); N, 8.26 (8.10). For $(Me_4N)_3[Eu(PYZ)_3]$, recrystallisation from a small volume of MeOH followed by slow evaporation yielded X-ray quality crystals, or alternately, by vapour diffusion with Et_2O overnight.

X-ray crystallography

X-ray crystallographic data for $(Me_4N)_3[Eu(PYZ)_3]{\cdot}4H_2O$ and $(Me_4N)_3[Eu(PYZ)_3]{\cdot}5MeOH$ was measured using an Oxford dual source SuperNova Diffractometer with Atlas CCD detector, employing Cu K_α radiation (1.54184 Å). Single crystals were coated in Paratone-N oil and mounted on a cryo loop for data collection, with external cooling at 130 K provided by an Oxford Cryostream LT device. Empirical absorption corrections were performed using a multifaceted crystal model and the ABSPACK routine within the CrysAlisPro software package. The structures were solved by direct methods and refined by the full-matrix least-squares method on F^2 with SHELXL-97,[12] using the WinGX software package.[13] For the $(Me_4N)_3[Eu(PYZ)_3]{\cdot}5MeOH$ complex, the crystals obtained were generally of low quality. After assigning all atoms, the residual electron density map showed anomalous peaks of 2–4 e Å^{-3} located within the Van der Waals radius of the Eu(III) cation, which may be due to unresolved disorder and/or absorption effects. All non-H atoms were refined anisotropically. H atoms of the pyrazine ligand and solvent molecules were positioned geometrically and refined using a riding model, with $U_{iso}(H)$ = 1.2 $U_{eq}(C/O)$. Diagrams of the resulting structures were created using Mercury.[14]

General photophysics

Solution concentrations for absorption and fluorescence measurements were *ca.* 10^{-5} to 10^{-6} M and 1.0 cm cells in quartz suprasil were used. UV-Visible absorption spectra were recorded with a Varian 50 double beam absorption spectrometer. Emission spectra in the visible region were acquired with a HORIBA Jobin Yvon IBH FluoroLog-311 spectrofluorimeter. Spectra were reference corrected for both the excitation light source variation (lamp and grating) and the emission spectral response (detector and grating). Emission spectra in the Near Infra-Red (NIR) region were measured using an Edinburgh Instruments FLS-920-STM spectrofluorimeter, equipped with a liquid N_2 cooled Ge detector (EI-L, Edinburgh Instruments). Quantum yields in solution were determined using optically dilute methods[15,16] and the equation:

$$\frac{\Phi_x}{\Phi_r} = \left[\frac{A_r(\lambda_r)}{A_x(\lambda_x)}\right]\left[\frac{I(\lambda_r)}{I(\lambda_x)}\right]\left[\frac{\eta_x^2}{\eta_r^2}\right]\left[\frac{D_x}{D_r}\right]$$

where A is the absorbance at excitation wavelength (λ), I is the excitation intensity at the same wavelength, η is the refractive index and D is the integrated luminescence signal. The

 This journal is © The Royal Society of Chemistry 2013

subscripts 'x' and 'r' refer to the sample and reference. In the visible region, a methanol solution of cresyl violet perchlorate was used as the reference[17] (Φ_r = 0.54.), while in the NIR region, a solution of [Yb(TTA)$(H_2O)_2$] (TTA = thenoytrifluoroacetylacetonate) in toluene was used as the reference[18] (Φ_r = 0.0035). The estimated error for these measurements is ±15%.

Time resolved and ultrafast spectroscopy

Time resolved luminescence experiments were performed using a nanosecond laser system. The tripled output of a Q-switched Nd:YAG (Continuum NY-61-10, Coherent) at 355 nm and 10 Hz was used to pump an OPO (Casix BBO, Shanghai Uniwave Technologies) tuned to 560 nm, which was frequency doubled using a type-1 BBO crystal to afford excitation pulses at 280 nm. These were focused on the sample using all quartz optics, and the emission from the sample was collected perpendicular to the excitation beam, collimated then refocused onto the entrance port of a 0.3 m triple grating monochromator (SpectraPro 300i, Acton Instruments). The detector was a standard photomultiplier (R928P, Hamamatsu), which was sampled directly using a 500 MHz digital oscilloscope (TDS520, Tektronix) using the sync out signal from the Q-switched Nd:YAG as the trigger. The instrument response function (IRF) for this experimental setup measured from the scattered excitation of a Ludox solution was *ca.* 12 ns. For lifetime measurements in the NIR region, we used a high speed InGaAs photodiode (DET10C, Thor Labs, Inc.) as the detector, the output of which was amplified using a high speed current amplifier (HCA-200 M-20 K-C, Laser Components, GmbH). Data analysis was performed using a commercially available software package (Igor, Version 6.1.2.1, Wavemetrics). Each trace contained at least 500 data points and was averaged over 128 laser shots. The quality of the fit was assessed using the calculated reduced chi-squared χ^2 function and by inspection of the weighted residuals, with an estimated error of ±10%.

Femtosecond transient absorption spectra were measured using a previously described setup.[19,20] Approximately 1 μJ of the output of an amplified Ti:sapphire system (Spitfire, Spectra Physics), delivering 800 nm pulses at 1 kHz, was focused into a CaF_2 window to generate the white light probe pulses. The remainder of the laser fundamental was frequency tripled in a non-collinear geometry to give pump pulses of approximately 1 μJ at 266 nm. The polarization of the pump was set to magic angle with respect to the probe pulses. The sample absorbance was *ca.* 0.2 over the 1 mm pathlength cell used, and the sample was continuously stirred mechanically. No important degradation was detected by absorption spectra taken prior to and after the TA measurements. The instrument response function (IRF) had a full width at half maximum (FWHM) of *ca.* 500 fs. All spectra were corrected for the chirp of the probe pulses, and the resulting time traces were analyzed globally using commercially available software (Igor, Version 6.1.2.1, Wavemetrics).

Table 1 Summary of X-ray crystal data for $(Me_4N)_3[Eu(PYZ)_3]\cdot 4H_2O$ and $(Me_4N)_3[Eu(PYZ)_3]\cdot 5MeOH$

	$(Me_4N)_3[Eu(PYZ)_3]\cdot 4H_2O$	$(Me_4N)_3[Eu(PYZ)_3]\cdot 5MeOH$
Formula	$C_{30}H_{50}N_9O_{16}Eu$	$C_{35}H_{62}N_9O_{17}Eu$
Formula weight	944.75 g mol^{-1}	1032.88 g mol^{-1}
Crystal system	Monoclinic	Monoclinic
Space group	$P2_1/c$	$P2_1/n$
a/Å	10.7804 (8)	10.8337 (5)
b/Å	20.6915 (16)	29.4292 (22)
c/Å	18.2029 (14)	15.1079 (14)
β/°	96.852 (6)	99.251 (7)
V/Å^3	4031.4 (5)	4754.16 (55)
Z	4	4
T/K	130	130
ρ_{calc}/g cm^{-3}	1.557	1.44
μ/mm^{-1}	11.822	10.089
Reflns measured	10 093	16 366
Unique reflns	5998	8935
Data/restraints/parameters	5998/13/541	8935/6/569
R_{int}	0.0453	0.0701
R_1 [$I > 2\sigma(I)$]	0.0846	0.1187
wR_2 (all data)	0.2099	0.3402
Goodness-of-fit on F^2	0.938	1.084
$\Delta\rho_{max,min}$/e Å^{-3}	1.98, −0.70	4.01, −1.36

Computational studies

Time-dependent density functional calculations (TD-DFT) were performed using the B3LYP/LANLD2Z basis set provided in Gaussian'03[21] with input coordinates derived from the crystal structure. Calculations were performed in the gas phase with no symmetry restraints.

Results and discussion

Synthesis and structure

The required $[Ln(PYZ)_3]^{3-}$ complexes were readily prepared by briefly refluxing the ligand and the appropriate $LnCl_3\cdot xH_2O$ salt (Ln = Eu, Yb; (x = 5), or Gd; (x = 6)) in MeOH, using a 30% solution of Me_4NOH as a base. The resulting products were isolated in analytically pure forms as their hydrated complexes. X-ray quality crystals for two pseudo-polymorphs of the Eu(III) complex were obtained, formulated as $(Me_4N)_3[Eu(PYZ)_3]\cdot 4H_2O$, when isolated by slow evaporation from a MeOH solution, or as $(Me_4N)_3[Eu(PYZ)_3]\cdot 5MeOH$, when isolated by vapour diffusion of Et_2O into a concentrated MeOH solution. A full summary of the crystallographic and structure refinement details is given in Table 1, and views of the unit cell contents and the complex anions are shown in Fig. 1.

The expected tridentate coordination mode of the PYZ^{2-} ligand with Eu(III) is observed experimentally in both cases, resulting in tricapped trigonal prismatic geometries at the metal, with D_3 symmetry. This coordination geometry is common for nine-coordinate (CN = 9) Ln(III) complexes with tris chelated tridentate ligands. The three coordinated pyrazine nitrogens (N1A, N1B, and N1C) form a plane perpendicular to the molecular C_3 axis, while two coordinated carboxylate

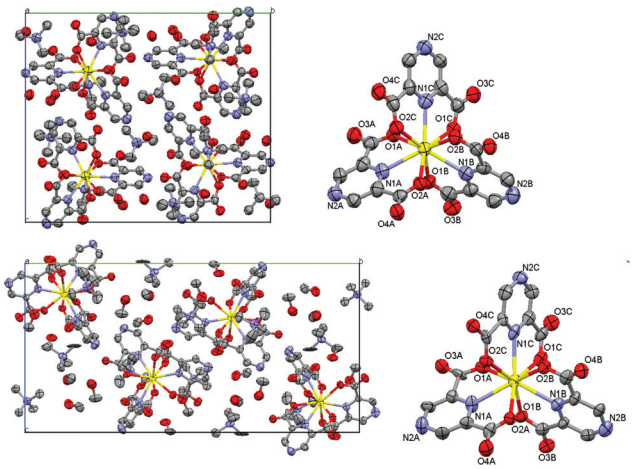

Fig. 1 (a) X-ray crystal structures for $(Me_4N)_3[Eu(PYZ)_3]\cdot 4H_2O$ (top) and $(Me_4N)_3[Eu(PYZ)_3]\cdot 5MeOH$ (bottom), as viewed along the crystallographic *a*-axis showing the unit cell contents (left), and (b) a view of the corresponding complex anions down the molecular C_3 axis (right) with selected atom labels (C, grey; O, red; N, blue; Eu, yellow; 50% probability ellipsoids shown, H atoms omitted for clarity).

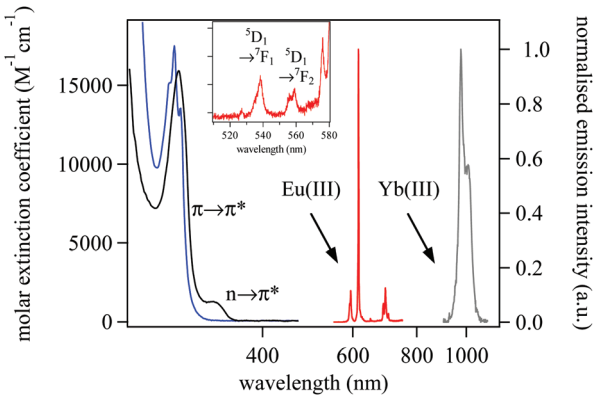

Fig. 2 Absorption spectra (left axis) of $[Eu(PYZ)_3]^{3-}$ (black) and $[Eu(DPA)_3]^{3-}$ (blue) and emission spectra (right axis, λ_{ex} = 275 nm) of $[Eu(PYZ)_3]^{3-}$ (red) and $[Yb(PYZ)_3]^{3-}$ (grey) in CH_3CN solution. Inset: Expansion of $[Eu(PYZ)_3]^{3-}$ emission spectrum showing $^5D_1 \rightarrow {}^7F_J$ peaks.

oxygen atoms from each of the three PYZ^{2-} ligands form two trigonal faces defined by the {O1A, O1B O1C} and {O2A, O2B, O2C} atoms. This results in upper and lower basal planes (see Fig. S1–S2, ESI†), which are almost parallel, being inclined by *ca.* ∠1.2° for $(Me_4N)_3[Eu(PYZ)_3]\cdot 4H_2O$ and by *ca.* ∠4.3° for $(Me_4N)_3[Eu(PYZ)_3]\cdot 5MeOH$. At the centre of these planes sits the Eu(III) cation, which is also located at the centre of three lateral planes defined by the {O2A, O1B, O2B, O1C}, {O1A, O2A, O1B, O2C} and {O1A, O2B, O1C, O2C} atoms (see Fig. S1 and S2, ESI†). For both complexes, a distortion of the ideal D_{3h} symmetry arises by a rotation of the trigonal faces with respect to each other about the C_3 axis, by *ca.* 15.0° for the $(Me_4N)_3[Eu(PYZ)_3]\cdot 4H_2O$ complex and by *ca.* 16.0° for $(Me_4N)_3[Eu(PYZ)_3]\cdot 5MeOH$. Similarly, for both compounds, the average of the Eu–N(pyz) bondlengths are almost identical at 2.52 ± 0.02 Å, and 2.50 ± 0.01 Å, respectively, while the averages of the coordinated oxygen atom bondlengths are slightly shorter at 2.43 Å ± 0.01 Å and 2.45 ± 0.03 Å, respectively. For $(Me_4N)_3[Eu(PYZ)_3]\cdot 4H_2O$, the remainder of the asymmetric unit is occupied by three Me_4N^+ counter cations, and four co-crystallized solvent water molecules (O1, O2, O3 and O4), which form numerous hydrogen bonding interactions with carboxylate oxygen atoms not coordinated to the metal (*e.g.* O1–H1···O4B = 1.98 Å, O4–H7···O4A = 1.91 Å). For $(Me_4N)_3[Eu(PYZ)_3]\cdot 5MeOH$, there are similarly three Me_4N^+ counter cations in the asymmetric unit, together with five co-crystallized solvent methanol molecules (O1–C19, O2–C20, O3–C21, O4–C22 and O5–C23), which also form several hydrogen bonding interactions with the free carboxylate oxygen atoms (*e.g.* O1–H1···O4C = 1.85 Å, O2–H2···O1B = 1.94 Å). A full list of these H-bonding interactions for both complexes, and additional views of the X-ray structures are given in the ESI (see Table S1, Fig. S3–S4†). Lastly, we note that the $(Me_4N)_3[Eu(PYZ)_3]\cdot 4H_2O$ complex reported herein shares very close structural similarity with an analogous $(Et_4N)_3[Eu(DPA)_3]\cdot 4H_2O$ complex previously reported by Harrowfield and Brayshaw.[22] In both cases, the lattice contains alternating columns of the Λ and Δ enantiomeric forms of the complex, related by the crystallographic mirror plane. The organic cations form additional columns in order to optimize electrostatic interactions, and the lattice water molecules are hydrogen bonded to the non-coordinated oxygen carboxylate atoms.

Solution photophysics

The absorption spectra of $[Ln(PYZ)_3]^{3-}$ (Ln = Eu, Yb, and Gd) in CH_3CN solution are essentially identical, and the Eu(III) complex is shown as an example in Fig. 2. Two absorption features are observed in the UV region, with a strong peak maximum at 274 nm (ε = 15 900 M^{-1} cm^{-1}), and a much smaller peak at 321 nm (ε = 1280 M^{-1} cm^{-1}). As previously reported,[5,9] we can assign these peaks to π–π* and n–π* features of the coordinated PYZ^{2-} dianion, respectively, which is supported by our TD-DFT calculations (*vide infra*). The assignment of the latter to an n–π* transition is also consistent with the observed red shift in CH_3CN solution, compared to the corresponding peak at *ca.* 308 nm we observed[5] as a shoulder in 0.1 M HEPES buffered aqueous solution (pH 7.4). Also shown in Fig. 2 is the absorption spectrum of the corresponding $[Eu(DPA)_3]^{3-}$ complex. In comparison to $[Eu(PYZ)_3]^{3-}$, we note for this complex the low energy n → π* band is completely absent and the absorption spectrum has a more well define vibrational structure, presumably due to the lack of additional underlying n → π* features.

Upon excitation at 275 nm or 320 nm, we observe sensitized metal based emission from the $[Ln(PYZ)_3]^{3-}$ complexes (Ln = Eu, Yb) in CH_3CN solution, as shown in Fig. 2. For Eu(III), the typical Eu(III) transitions of the $^5D_0$ excited state to the ground state ^7F_J manifold are evident, with peak maxima located at *ca.* 580 (J = 0), 593 (J = 1), 615 (J = 2), 649 (J = 3) and 688, 693, 703 nm (J = 4). At slightly higher energy, we also observe additional weak (but nonetheless clearly resolved) emission peaks which we can assign to the Eu(III) $^5D_1 \rightarrow {}^7F_J$ transitions,

 This journal is © The Royal Society of Chemistry 2013

with peak maxima apparent at *ca.* 527 (J = 0), 538 (J = 1), and 557 nm (J = 2), which are shown in the inset of Fig. 2. For the Yb(III) complex, a single sharp peak at 976 nm and weaker shoulder at 1008 nm was observed corresponding to the $^2F_{5/2} \rightarrow {}^2F_{7/2}$ transition of the Yb(III) cation.

For the $[Eu(PYZ)_3]^{3-}$ and $[Eu(DPA)_3]^{3-}$ complexes, we have measured the time resolved decay profiles of the $^5D_0 \rightarrow {}^7F_2$ transition at *ca.* 615 nm. For both complexes, the observed lifetimes gave excellent fits to a simple monoexponential decay function, which, based on the similarity to the lifetimes we previously determined[5] in the solid state, we can assign to the tris $[Eu(L)_3]^{3-}$ complexes (L = DPA^{2-} or PYZ^{2-}). These results establish that the $[Eu(L)_3]^{3-}$ complexes are stable in CH_3CN solution at micromolar concentrations, which differs from the situation in 0.1 M HEPES buffered aqueous solution (pH = 7.4), where competitive hydrolysis below mM concentrations was evident, in particular for $[Eu(PYZ)_3]^{3-}$. Similarly, for the $[Yb(PYZ)_3]^{3-}$ and $[Yb(DPA)_3]^{3-}$ complexes, we were able to measure monoexponential decays for the $^2F_{5/2}$ excited state at 980 nm, with lifetime values of 27.2 μs and 22.2 μs, respectively (see Fig. 3 and Fig. S5, ESI†). For the latter, this lifetime is longer than that reported[6] in aqueous solution ($\tau_{obs} \sim 2.23 \pm 0.01$ μs), which can be expected due to the absence of non-radiative quenching by solvent H_2O molecules.[26]

Interestingly, using our nanosecond laser setup which affords *ca.* 8 ns excitation pulses, we were also able to measure the rise time for population of the $^5D_0$ excited state of the Eu(III) cation for both $[Eu(PYZ)_3]^{3-}$ (Fig. 3) and $[Eu(DPA)_3]^{3-}$ (Fig. S5, ESI†). The resulting fit to a monexponential rise gave a value of τ_{rise} = 1.43 ± 0.05 μs, which was identical for both compounds. Similarly, by monitoring the weak emission of the $^5D_1 \rightarrow {}^7F_1$ transition at 538 nm, we could measure the corresponding decay of the $^5D_1$ excited state, which gave the same value. Hence, for both complexes, the sensitization process for the Eu(III) cation involves (at least to some extent) internal conversion from the intermediate $^5D_1$ excited state located at *ca.* 19 028 cm^{-1}. These results are consistent with those of de Sá *et al.*,[23] who have argued that, based on the selection rules for the direct and exchange Coulombic interactions, direct energy transfer to the $^5D_0$ level is forbidden, and an excellent candidate for involvement in the exchange energy transfer mechanism is instead the $^5D_1$ manifold. The identical values we obtain for the rise and decay of the $^5D_0$ and $^5D_1$ electronic states for both $[Eu(PYZ)_3]^{3-}$ and $[Eu(DPA)_3]^{3-}$ can be rationalized since these two complexes have almost identical coordination geometries.

We have quantifed the intensity of the Ln(III) emission *via* luminescence quantum yield measurements with the resulting data summarized in Table 2 (see also Fig. S6, ESI†). For the $[Eu(PYZ)_3]^{3-}$ complex, the resulting value of Φ_{total} was 61.8 ± 4.7%, which is only marginally higher than the value for $[Eu(DPA)_3]^{3-}$ measured under identical experimental conditions. Indeed, as we noted previously in the solid state,[5] these results are essentially identical within experimental error, which suggests the anticipated enhancement in Φ_{total} we sought by substitution of the DPA^{2-} ligand with PYZ^{2-} was not realized

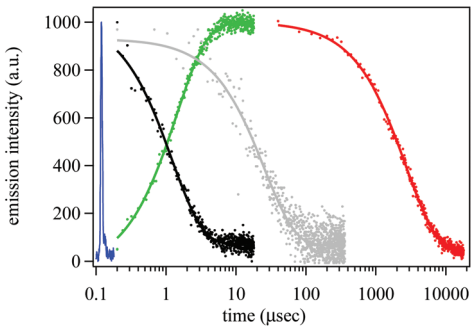

Fig. 3 Observed decays of $^5D_0$ (red, λ_{em} = 615 nm) and $^5D_1$ excited states (black, λ_{em} = 538 nm) of $[Eu(PYZ)_3]^{3-}$ and $^2F_{5/2}$ excited state (grey, λ_{em} = 980 nm) of $[Yb(PYZ)_3]^{3-}$ in CH_3CN solution. Corresponding rise of the Eu(III) $^5D_0$ excited state (green, λ_{em} = 615 nm). Monoexponential fits to the data are shown as solid lines, and the instrument response is shown in blue. Note: $\log_{10}$ scale used on x-axis for clarity.

experimentally. However, in the case of the corresponding Yb(III) complexes, we do note a dramatic increase in the observed Near Infra-Red (NIR) emission intensity at *ca.* 1 μm, which is more than twice as high with PYZ^{2-} than with DPA^{2-}.

Using the experimental luminescence lifetimes, and adopting the methods proposed by Werts *et al.*,[24] and Beeby *et al.*,[25] and recently verified by Bünzli *et al.*,[6] we have calculated the radiative lifetime, τ_{rad}, from the corrected emission spectrum for the $[Eu(PYZ)_3]^{3-}$ and $[Eu(DPA)_3]^{3-}$ complexes using the equation:

$$k_r = \frac{1}{\tau_{rad}} = A_{MD,0}\eta^3\left(\frac{I_{tot}}{I_{MD}}\right)$$

where η is the refractive index, $A_{MD,0}$ is the emission probability of the $^5D_0 \rightarrow {}^7F_1$ transition (14.65 s^{-1}), and I_{tot} and I_{MD} are the integrated areas of the entire spectrum and the $^5D_0 \rightarrow {}^7F_1$ (MD) transition, respectively. For the $[Yb(DPA)_3]^{3-}$ complex, the solubility of the complex in CH_3CN was not sufficient to experimentally determine the radiative lifetime.[24] Instead, we have used the known literature value of τ_{rad} = 1.31 ms for this complex reported[6] by Bünzli *et al.*, We have corrected this value for the difference in refractive index of H_2O *vs.* CH_3CN solvent, yielding a value of 1.29 ms, although this value must be taken with some caution, since it is known[26,27] that the radiative lifetime can sometimes be influenced by other second sphere effects.

The remaining important photophysical parameters, including the intrinsic quantum yield for metal centered luminescence (*e.g.* for direct 4f–4f absorption, or in the case of 100% sensitization efficiency), Φ_{Ln}, can be derived using the following equations:

$$k_{nr} = \frac{1}{\tau_{obs}} - k_r \qquad \Phi_{Ln} = \frac{k_r}{(k_r + k_{nr})} \qquad \eta_{sens} = \frac{\Phi_{total}}{\Phi_{Ln}}$$

and these parameters are summarized in Table 2 for the $[Ln(PYZ)_3]^{3-}$ and $[Ln(DPA)_3]^{3-}$ complexes (Ln = Eu, Yb).

Our analysis reveals that, as we reported previously in the solid state,[5] the radiative decay rate constants, and hence

Table 2 Summary of absorption and luminescence properties for $[Ln(PYZ)_3]^{3-}$ and $[Ln(DPA)_3]^{3-}$ (Ln = Eu, Yb) in CH_3CN solution

Complex	λ_{max} (nm)	ε_{max} (M^{-1} cm^{-1})	Φ_{total}[a,b] (%)	τ_{obs} (ms)	τ_{rad} (ms)	k_r (ms^{-1})	k_{nr} (ms^{-1})	Φ_{Ln} (%)	η_{sens} (%)
$[Eu(PYZ)_3]^{3-}$	274	15 900	61.8[a]	2.71	3.85	0.26	0.11	70.2	88.0
	321	1 280							
$[Eu(DPA)_3]^{3-}$	277	13 530	60.4[a]	2.25	3.70	0.27	0.18	60.6	99.6
	269	17 480							
$[Yb(PYZ)_3]^{3-}$	274	16 120	0.51[b]	0.0272	1.29	0.78	36.0	2.1	24.1
	320	1310							
$[Yb(DPA)_3]^{3-}$	277	13 640	0.23[c]	0.0222	1.29	0.78	44.3	1.7	13.3
	269	17 600							

[a] Relative values *vs.* cresyl violet perchlorate in methanol, (Φ_{ref} = 54%). [b] Relative value *vs.* $[Yb(TTA)_3(H_2O)_2]$ in toluene, (Φ_{ref} = 0.35%). [c] Relative value *vs.* $[Yb(PYZ)_3]^{3-}$.

radiative lifetimes of the $[Eu(PYZ)_3]^{3-}$ and $[Eu(DPA)_3]^{3-}$ complexes are very similar (within 5%), which can be expected, since both share an essentially identical coordination environment. For the $[Yb(PYZ)_3]^{3-}$ complex, we assume a value of τ_{rad} = 1.29 ms, identical to that of the $[Yb(DPA)_3]^{3-}$ complex for the same reasons. In accordance with Bünzli's previously reported results[6] using the $[Eu(DPA)_3]^{3-}$ complex, we note a similar trend in the radiative lifetime of $[Eu(PYZ)_3]^{3-}$, with the value of τ_{rad} significantly longer in solution compared to the solid state (3.85 ms *vs.* 2.66 ms). This illustrates the radiative lifetime, and hence the intrinsic quantum yield, Φ_{Eu}, is strongly dependent on the metal ion's environment and also the refractive index of the medium. For the $[Eu(PYZ)_3]^{3-}$ complex, the non-radiative decay rate constant is considerable smaller compared to $[Eu(DPA)_3]^{3-}$. We attribute this decrease in k_{nr}, at least in part, to the loss of three –CH oscillators in close proximity (~5.2 Å) to the Eu(III) cation for the $[Eu(PYZ)_3]^{3-}$ complex, since these groups have a known non-radiative quenching effect on metal centered luminescence. The decrease we observe of *ca.* 0.023 ms^{-1} per –CH oscillator is similar to the value estimated by Beeby *et al.*,[28] for an individual alkyl –CH oscillator of 0.028 ms^{-1}, obtained from luminescence studies with selectively deuterated $[Eu(DOTA)(H_2O)]$ complexes.

As a result of the differences in the non-radiative decay rate constant, the metal based quantum yield, Φ_{Eu}, is calculated to be higher for the $[Eu(PYZ)_3]^{3-}$ complex. However, this increase is offset by a lower value of the sensitization efficiency, η_{sens}, by *ca.* 10%, resulting in almost identical Φ_{total} values for the Eu(III) complexes. For the Yb(III) complexes, we note the ratio of the intrinsic quantum yields, Φ_{Yb}, would yield an expected relative enhancement of 22.5% in Φ_{total} for $[Yb(PYZ)_3]^{3-}$, which is lower than the *ca.* 120% observed experimentally. This suggests that the observed increase in Φ_{total} cannot be attributed solely to the difference in k_{nr}, and indeed, we instead also calculate a more efficient η_{sens} value of 24.1% for $[Yb(PYZ)_3]^{3-}$, compared to 13.3% for $[Yb(DPA)_3]^{3-}$.

In order to rationalize the differences in sensitization efficiencies with Eu(III), and to more adequately understand the enhanced NIR luminescence intensity of the Yb(III) complexes with PYZ^{2-} compared to DPA^{2-}, we have prepared the Gd(III) complexes. The Gd(III) cation has a similar size and atomic weight compared with the other lanthanides, but lacks low energy metal centred electronic energy levels, making complexes of this metal cation useful for estimating the position of low energy ligand-centered triplet states (T_1) *via* their phosphorescence. Measurements were performed at room temperature, and 77 K in 1 : 1 (v/v) MeOH : EtOH, and resulting spectra are shown in Fig. 4.

At room temperature, we observe a weak signal at 31 150 ± 100 cm^{-1} (*ca.* 321 nm), which we assign to residual S_1 (n–π*) fluorescence of the complexed ligand. Upon cooling to 77 K, and using a 10 μs phosphorescence delay, an intense, red shifted and unstructured emission band appears between *ca.* 380–500 nm, which we attribute to the coordinated PYZ^{2-} ligand. The lowest energy zero phonon (ν_{0-0}) band of this state was estimated by spectral deconvolution of the 77 K luminescence signal into a series of overlapping Gaussian functions, yielding a value of 24 840 ± 100 cm^{-1} for the lowest energy T_1 state.

A resulting partial energy level diagram, summarising the important ligand based and metal based energy levels can be constructed, as shown in Fig. 5. We note in particular that the energy difference between the PYZ^{2-} T_1 state and the Yb(III) $^2F_{5/2}$ acceptor level is *ca.* 14 400 cm^{-1}, compared to *ca.* 16 600 cm^{-1} for DPA^{2-}. To paraphrase, the position of the T_1 state for $[Gd(PYZ)_3]^{3-}$ is *ca.* 2200 cm^{-1} lower in energy compared to the known value of the $[Gd(DPA)_3]^{3-}$ complex.[6] Based on the energy gap law, which states that the probability of

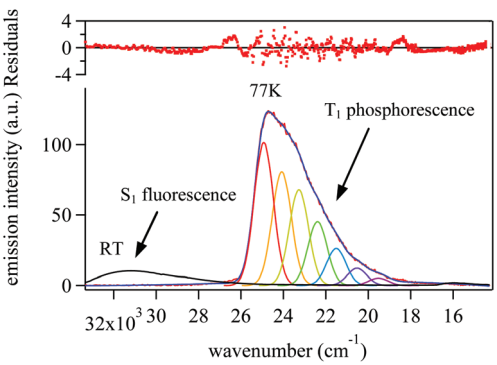

Fig. 4 Emission spectrum (λ_{ex} = 275 nm) for $[Gd(PYZ)_3]^{3-}$ at room temperature (black) and 77 K (red) in 1 : 1 EtOH : MeOH glassing solvent, and fit to a series of overlapping Gaussian functions (see text).

 This journal is © The Royal Society of Chemistry 2013

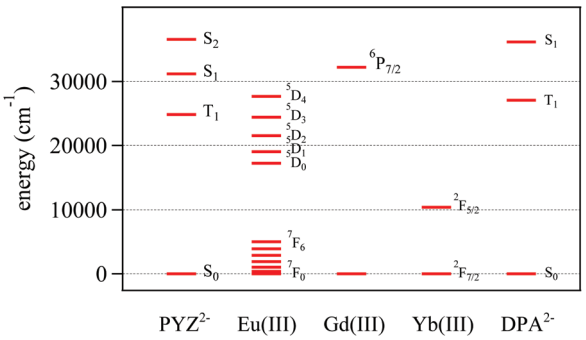

Fig. 5 Energy level diagram showing ligand based and metal based electronic energy levels for $[Ln(PYZ)_3]^{3-}$ and $[Ln(DPA)_3]^{3-}$ complexes.

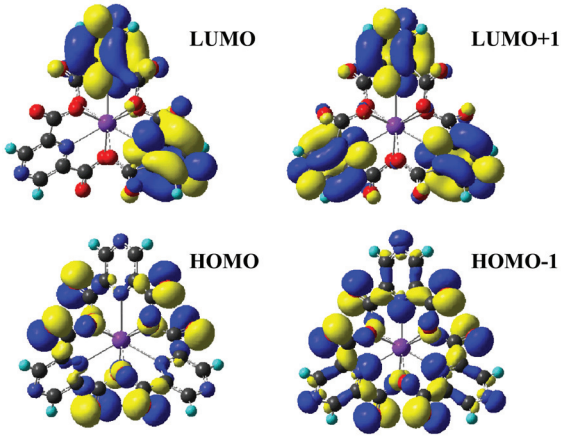

Fig. 6 Optimized output geometry and molecular orbital diagrams for a model $[Y(PYZ)_3]^{3-}$ complex obtained from TD-DFT calculations (B3LYP/LANLD2Z).

intramolecular energy transfer between two electronic states is inversely proportional to their energy difference,[29] this should result in a more efficient energy transfer to the Yb(III) cation for complexes with PYZ^{2-}, which agrees with our observations involving the calculated values of the sensitization efficiency, η_{sens}. Hence, in addition to the differences in the non-radiative decay rate constant which we noted earlier may account for as much as a 22.5% increase in the luminescence intensity, the remainder of the experimentally observed increase can be attributed to more efficient sensitization, as a result of the lower T_1 energy of Ln(III) complexes with the PYZ^{2-} anion.

Electronic structure calculations

To support our experimental results, we have undertaken DFT calculations for a simplified model system, replacing the Ln(III) with diamagnetic Y(III) to avoid computationally expensive calculations involving an open shell 4f metal. The Y(III) cation has an identical charge and similar ionic radius to the middle lanthanides,[30] and we have found approaches such as this to be useful for understanding the electronic structure of the lowest excited singlet and triplet states of complexed organic ligands.[31] Corresponding electronic structure calculations determined *via* TD-DFT techniques are summarized in the ESI (see Table S2†), and relevant molecular orbitals involving in these transitions are depicted in Fig. 6.

Most importantly, for the $[Y(PYZ)_3]^{3-}$ complex, the lowest energy T_1 state is predicted to be located at 23 091 cm^{-1}, which is very similar (within 10%) to the value of *ca.* 24 840 cm^{-1} we determined experimentally for the $[Gd(PYZ)_3]^{3-}$ complex at 77 K. Analysis of the relevant molecular orbitals involved with this transition reveal it to be of mixed parentage, with *ca.* 38% attributable to transitions from the HOMO − 1 → LUMO and HOMO − 1 → LUMO + 1, which, as shown in Fig. 6, demonstrates clearly discernable n → π* character for this transition, involving lone pairs of the non-coordinated pyrazine N atom and the aromatic π system.

Transient absorption measurements

Lastly, in an effort to rationalize the differences observed for the sensitization efficiencies, η_{sens}, of the Eu(III) and Yb(III) complexes, we have undertaken ultrafast transient absorption (TA) experiments on the femtosecond timescale. The resulting TA spectra are shown in Fig. 7, and the extracted decay constants obtained from global analysis of these spectra (see also Fig. S7–S14, ESI†) are summarized in Table 3.

The TA spectrum of H_2DPA reveals a broad structureless band in the visible region with a maximum at *ca.* 440 nm, which we assign to an $S_n \leftarrow S_1$ transition. This signal decays very rapidly ($\tau_1 \sim 20$ ps) yielding a longer lived signal which decays towards zero, with a broad feature in the UV region, tailing into the observable spectral window from *ca.* 370–670 nm. For H_2PYZ, the TA spectrum is quite similar with a broad rapidly decaying band ($\tau_1 \sim 260$ ps) centred at *ca.* 440 nm, similarly assigned to an $S_n \leftarrow S_1$ transition. However, an additional shoulder at *ca.* 490 nm with the same decay constant is visible at lower energy.

Upon complexation with Ln = Gd, Eu, and Yb, we note that the shape of the TA spectra remain essentially unchanged for both the $[Ln(DPA)_3]^{3-}$ and $[Ln(PYZ)_3]^{3-}$ complexes. However, the decay constants associated with these bands are considerably different, with values as summarized in Table 3. In particular, it is readily apparent that the S_1 excited state lifetimes are all reduced upon complexation with the lanthanide cation. This decrease can be attributed to an enhanced intersystem crossing (increased k_{isc}) in the presence of the metal ion, together with changes in other non-radiative processes, with overall increase in rate constants compared to free ligands on the order of 10^8 to 10^{11} s^{-1}, as summarized in Table 3. For the complexes with DPA^{2-}, we note that this difference is only very slight. Additionally, we note that while the S_1 decay times for the Yb(III) and Gd(III) complexes with PYZ^{2-} are similar, the lifetime observed for the $[Eu(PYZ)_3]^{3-}$ complex is smaller, suggesting an additional quenching mechanism may exist. Similarly, for $[Eu(DPA)_3]^{3-}$, the decay time is also much smaller than for the corresponding Gd(III) complex. However, in this case, the S_1 decay time of the Yb(III) complex is also smaller than that of $[Gd(DPA)_3]^{3-}$. This suggests the decrease may be due to partial deactivation by a low energy charge

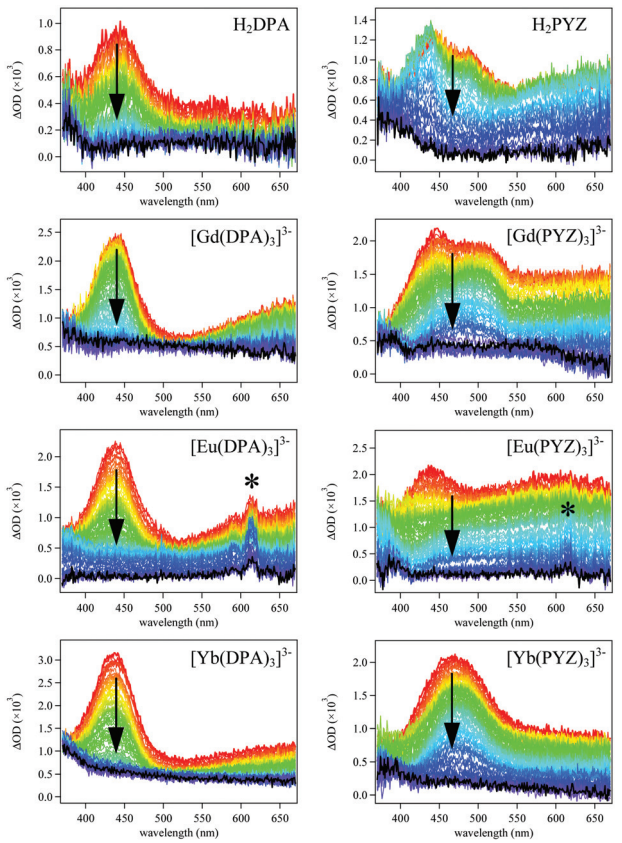

Fig. 7 Transient absorption spectra measured at various time delays (from red (~6 ps) to black (~1.7 ns)) after photoexcitation for H_2DPA (left), H_2PYZ (right), $[Ln(PYZ)_3]^{3-}$ and $[Ln(DPA)_3]^{3-}$ complexes (Ln = Gd, Eu, Yb from top to bottom). Features marked by an asterisk for Eu(III) are an artefact due to errors subtracting the intense metal emission.

transfer (^{1}MLCT) state, more accessible for the DPA^{2-} complexes due to their higher S_1 excited state singlet energies.

In addition to the observed differences in the S_1 decay times, we note that for both Eu(III) complexes, the longer lived feature in the UV region which we assign to a $T_n \leftarrow T_1$ absorption feature has decayed completely to zero in the observable time delay window. As a result, for these complexes, we are able to also estimate the lifetime of the lowest energy excited T_1 triplet states, arriving at lifetime values of τ_2 = 320 ps and $\tau_2 \approx$ 1600 ps for the $[Eu(DPA)_3]^{3-}$ and $[Eu(PYZ)_3]^{3-}$ complexes, respectively. Assuming that the radiative rate constants of the T_1 states are similar for complexes with Eu(III) and Gd(III), and using an estimate based on other Gd(III) complexes[32,33] of *ca.* 10–100 μ s for the T_1 lifetime of the latter at room temperature, we can then estimate rate constants for energy transfer from the T_1 state to the metal, using the difference in reciprocal lifetimes. We equate these values to be *ca.* 6.2×10^8 s^{-1} and 3.1×10^9 s^{-1}, respectively for $[Eu(PYZ)_3]^{3-}$ and $[Eu(DPA)_3]^{3-}$. Hence, for $[Eu(DPA)_3]^{3-}$, the k_{eet} rate constant is *ca.* 5 times faster than $[Eu(PYZ)_3]^{3-}$, which we propose is the reason for higher sensitization efficiency (η_{sens}) that we observed.

Table 3 Summary of S_1 and T_1 state decay kinetics for H_2DPA, H_2PYZ, $[Ln(PYZ)_3]^{3-}$ and $[Ln(DPA)_3]^{3-}$ complexes (Ln = Gd, Eu, Yb) observed by fs TA measurements (λ_{ex} = 266 nm)

Compound	τ_1 (S_1) (ps)	Δk_{ISC} ($+\Delta k_{nr}$)	τ_2 (T_1) (ps)
H_2PYZ	260	N/A	>2000
$[Gd(PYZ)_3]^{3-}$	33	2.6×10^{10} s^{-1}	>2000
$[Eu(PYZ)_3]^{3-}$	25	3.6×10^{10} s^{-1}	1600
$[Yb(PYZ)_3]^{3-}$	36	2.4×10^{10} s^{-1}	>2000
H_2DPA	20	N/A	>2000
$[Gd(DPA)_3]^{3-}$	19.9	2.5×10^{8} s^{-1}	>2000
$[Eu(DPA)_3]^{3-}$	4	2.2×10^{11} s^{-1}	320
$[Yb(DPA)_3]^{3-}$	6	1.2×10^{11} s^{-1}	>2000

Conclusions

We have demonstrated that the pyrazine-2,6-dicarboxylate dianion (PYZ^{2-}) is an excellent sensitizer for Ln(III) luminescence, forming highly emissive $[Ln(PYZ)_3]^{3-}$ complexes (Ln = Eu, Yb) which have good stability and solubility in non-aqueous solution. For Eu(III), while the intrinsic quantum yield of the metal centre, Φ_{Eu}, is enhanced compared to the well know complexes with the structurally analogous pyridine-2,6-dicarboxylate (DPA^{2-}) dianion, the overall quantum yields, Φ_{total}, are almost identical due to a decrease in the sensitization efficiency, η_{sens}. By contrast, with Yb(III), both the intrinsic metal centred quantum yield, Φ_{Yb}, and the sensitization efficiency, η_{sens}, are improved, resulting in complexes which are significantly more emissive in the Near Infra-Red (NIR) region. We have related the observed differences in emission behaviour principally to the differing energetic position of the relevant lowest energy T_1 triplet states, and using femtosecond transient absorption spectroscopy, we are also able to correlate the decrease in sensitization efficiency for the $[Eu(PYZ)_3]^{3-}$ complex to a less efficient energy transfer step. By contrast, for Yb(III), we suggest the enhanced η_{sens} is due to a faster energy transfer step, in accordance with our expectations based on the energy gap rule. The rates of intersystem crossing in Ln(III) complexes were found to be ultrafast, as expected, and account for the dominant singlet relaxation pathway. We are currently undertaking similar transient absorption experiments with a series of Ln(III) terpyridine derivatives on both the femtosecond and longer nanosecond timescales, to examine the generality and applicability of these results towards designing more highly emissive Ln(III) compounds.

Acknowledgements

Financial support from the Australian Research Council (ARC-DP0879996) and the European Research Executive Agency (REA-PIIF-GA-2010-275606) are gratefully acknowledged. EGM acknowledges financial support from the European Science Foundation in the form of a Short Visit Travel Grant (ESF-DYNA-3147). The authors also wish to thank Dr Robert Gable (University of Melbourne) for assistance with the X-ray crystallography.

This journal is © The Royal Society of Chemistry 2013

References

1 E. Soini and T. Lövgren, *CRC Crit. Rev. Anal. Chem.*, 1987, **18**, 105.
2 R. Pal, D. Parker and L. C. Costello, *Org. Biomol. Chem.*, 2009, **7**, 1525.
3 L. N. Krasnoperov, S. A. E. Marras, M. Kozlov, L. Wirpsza and A. Mustaev, *Bioconjugate Chem.*, 2010, **21**, 319.
4 A. Beeby, S. W. Botchway, I. M. Clarkson, S. Faulkner, A. W. Parker, D. Parker and J. A. G. Williams, *J. Photochem. Photobiol., B.*, 2000, **57**, 83.
5 E. G. Moore, *Dalton Trans.*, 2012, 5272.
6 A. Aebischer, F. Gumy and J.-C. G. Bünzli, *Phys. Chem. Chem. Phys.*, 2009, **11**, 1346.
7 A. S. Chauvin, F. Gumy, D. Imbert and J.-C. G. Bünzli, *Spectrosc. Lett.*, 2004, **37**, 517.
8 A. S. Chauvin, F. Gumy, D. Imbert and J.-C. G. Bünzli, *Spectrosc. Lett.*, 2007, **40**, 517.
9 I. Yamazaki, T. Murao, T. Yamanaka and K. Yoshihara, *Faraday Discuss. Chem. Soc.*, 1983, **75**, 395.
10 F. Weygand, *Chem. Ber.*, 1940, **73**, 1259.
11 H. I. X. Mager and W. Berends, *Recueil*, 1958, **77**, 827.
12 G. Sheldrick, *SHELX-97 Program for Crystal Structure Solution*, University of Göttingen, Germany, 1997.
13 L. J. Farrugia, *J. Appl. Crystallogr.*, 1999, **32**, 837.
14 C. F. Macrae, P. R. Edgington, P. McCabe, E. Pidcock, G. P. Shields, R. Taylor, M. Towler and J. Van de Streek, Mercury: visualization and analysis of crystal structures, *J. Appl. Crystallogr.*, 2006, **39**, 453.
15 G. A. Crosby and J. N. Demas, *J. Phys. Chem.*, 1971, **75**, 991.
16 G. Angulo, G. Grampp, J. Grilj, P. Jacques, S. Landgraf and A. Rosspeintner, *J. Photochem. Photobiol., A.*, 2008, **199**, 204.
17 D. F. Eaton, *Pure Appl. Chem.*, 1988, **60**, 1107.
18 M. P. Tsvirko, S. B. Meshkova, V. Y. Venchikov and D. V. Bol'shoi, *Opt. Spectrosc. (Engl. Transl.)*, 1999, **87**, 866.
19 G. Duvanel, N. Banerji and E. Vauthey, *J. Phys. Chem. A*, 2007, **111**, 5361.
20 N. Banerji, G. Duvanel, A. Perez-Velasco, S. Maity, N. Sakai, S. Matile and E. Vauthey, *J. Phys. Chem. A.*, 2009, **113**, 8202.
21 M. J. Frisch, G. W. Trucks, H. B. Schlegel, G. E. Scuseria, M. A. Robb, J. R. Cheeseman, J. A. Montgomery Jr., T. Vreven, K. N. Kudin, J. C. Burant, J. M. Millam, S. S. Iyengar, J. Tomasi, Vo. Barone, B. Mennucci, M. Cossi, G. Scalmani, N. Rega, G. A. Petersson, H. Nakatsuji, M. Hada, M. Ehara, K. Toyota, R. Fukuda, J. Hasegawa, M. Ishida, T. Nakajima, Y. Honda, O. Kitao, H. Nakai, M. Klene, X. Li, J. E. Knox, H. P. Hratchian, J. B. Cross, V. Bakken, C. Adamo, J. Jaramillo, R. Gomperts, R. E. Stratmann, O. Yazyev, A. J. Austin, R. Cammi, C. Pomelli, J. W. Ochterski, P. Y. Ayala, K. Morokuma, G. A. Voth, P. Salvador, J. J. Dannenberg, V. G. Zakrzewski, S. Dapprich, A. D. Daniels, M. C. Strain, O. Farkas, D. K. Malick, A. D. Rabuck, K. Raghavachari, J. B. Foresman, J. V. Ortiz, Q. Cui, A. G. Baboul, S. Clifford, J. Cioslowski, B. B. Stefanov, G. Liu, A. Liashenko, P. Piskorz, I. Komaromi, R. L. Martin, D. J. Fox, T. Keith, M. A. Al-Laham, C. Y. Peng, A. Nanayakkara, M. Challacombe, P. M. W. Gill, B. Johnson, W. Chen, M. W. Wong, C. Gonzalez and J. A. Pople, *GAUSSIAN 03 (Revision C.02)*, Gaussian, Inc., Wallingford, CT, 2004.
22 P. A. Brayshaw and J. M. Harrowfield, *Acta Crystallogr. Sect. C: Cryst. Struct. Commun.*, 1995, **51**, 1799.
23 G. F. De Sá, O. L. Malta, C. de Mello Donegá, A. M. Simas, R. L. Longo, P. A. Santa-Cruz and E. F. da Silva Jr., *Coord. Chem. Rev.*, 2000, **196**, 165.
24 M. H. V. Werts, R. T. F. Jukes and J. W. Verhoeven, *Phys. Chem. Chem. Phys.*, 2002, **4**, 1542.
25 A. Beeby, L. M. Bushby, D. Maffeo and J. A. G. Williams, *J. Chem. Soc., Dalton Trans.*, 2002, 48.
26 N. Shavaleev, R. Scopelliti, F. Gumy and J.-C. G. Bünzli, *Inorg. Chem.*, 2009, **48**, 7937.
27 F. Artizzu, F. Quochi, M. Saba, D. Loche, M. L. Mercuri, A. Serpe, A. Mura, G. Bongiovanni and P. Deplano, *Dalton Trans.*, 2012, 13147.
28 A. Beeby, I. M. Clarkson, R. S. Dickins, S. Faulkner, D. Parker, L. Royle, A. S. de Sousa, J. A. G. Williams and M. Woods, *J. Chem. Soc., Perkin Trans. 2*, 1999, 493.
29 B. Wardle, *Principles and Applications of Photochemistry*, John Wiley & Sons, Ltd, West Sussex, UK, 2009.
30 R. D. Shannon, *Acta Crystallogr., Sect. A: Cryst. Phys., Diffr., Theor. Gen. Cryst.*, 1976, **32**, 751.
31 A. D'Aleo, J. Xu, E. G. Moore, C. J. Jocher and K. N. Raymond, *Inorg. Chem.*, 2008, **47**, 6109.
32 S. I. Klink, L. Grave, D. N. Reinhoudt, F. C. J. M. van Veggel, M. H. V. Werts, F. A. J. Geurts and J. W. Hofstraat, *J. Phys. Chem. A.*, 2000, **104**, 5457.
33 A. Beeby, S. Faulkner, D. Parker and J. A. G. Williams, *J. Chem. Soc., Perkin Trans. 2*, 2001, 1268.

This journal is © The Royal Society of Chemistry 2013